Polymer 51 (2010) 5585–5591

Contents lists available at ScienceDirect

Polymer

journal homepage: www.elsevier.com/locate/polymer

Real-time investigation of crystallization in nylon 6-clay nano-composite probed by infrared spectroscopy

Takaya Ishisue [a], Masami Okamoto [a,*], Kohji Tashiro [b]

[a] Advanced Polymeric Nanostructured Materials Engineering, Graduate School of Engineering, Toyota Technological Institute, 2-12-1 Hisakata, Tempaku, Nagoya 468 8511, Japan
[b] Department of Future Industry-oriented Basic Science and Materials, Graduate School of Engineering, Toyota Technological Institute, 2-12-1 Hisakata, Tempaku, Nagoya 468 8511, Japan

ARTICLE INFO

Article history:
Received 6 April 2010
Received in revised form
23 July 2010
Accepted 14 September 2010
Available online 21 September 2010

Keywords:
Nano-composites
Crystallization
Polymorph

ABSTRACT

Via time-resolved FTIR, we examined the real-time investigation of the structural change in molecular chain of nylon 6 during crystallization of neat nylon 6 and the corresponding nano-composite (N6C3.7) having fully exfoliated structure. The neat nylon 6 predominantly formed α-phase in the crystallization temperature (T_c) range of 155–195 °C. For N6C3.7 crystallization at low T_c range of 150–168 °C, where the network structure formed by the dispersed clay particles still affected chain folding of nylon 6, the formation of the γ-phase was dominant. The crystallization took place so rapidly (less than 1 s) without induction time of crystallization. At high T_c range (=177–191 °C), the stable growth of the α-phase crystal coexisting with γ-phase occurred in N6C3.7 crystallization. The growth mechanism in the subsequent crystallization processes (amides IIIα and IIIγ) was virtually the same in both N6C3.7 and neat nylon 6.

1. Introduction

Nylon 6 was crystallized extensively in the γ-form in the nano-composites [1–13]. The phase is preferentially crystallized in the γ polymorph in the presence of the montmorillonite (MMT) and/or the organically modified MMT (organo-clay). They reported that similar crystal lattices between clay and the γ polymorph, and the large flat surface of the clay are the key factors to interact between polymer and inorganic materials. The epitaxial crystallization was also revealed from the transmission electron microscopic images [9,12]. That is, the clay surface induces kinetically favored γ-phase formation. In the pseudo-hexagonal γ-form crystals, the molecular chains have to twist away from the zigzag planes to form hydrogen bonds among the parallel chains in the crystals giving rise to lesser inter-chain interactions compared with the monoclinic α-form, which are all-trans and packed in more stable antiparallel-chain arrangement of hydrogen bonds [13].

Besides the nucleating effect, the clay surfaces (silicate layers) can also clearly retard the crystal growth process [6,14]. The clay-induced reduction of the crystallization rate is due to the disruption of lamella growth by the well dispersed MMT particles [6]. Hominga et al. [15] suggested that the silicate layers hinder the diffusion of polymer chains to the crystal growth front and impurity migration away from the growth front takes place. Miltner et al. [16] reported that the interaction between nylon 6 and MMT reduce the mobility of the polymer chain which benefits to form the γ-phase, depending on the nature of the organo-clay (MMT-intercalant). Furthermore, once a percolated network of the dispersed MMT particles is formed, the networks retard crystalline capability as reported by our previous paper [12] and Wang et al. [17].

In our previous paper [12], we have shown that the lamellar growth of the γ-phase crystal took place on both sides of the dispersed MMT particles. The overall crystallization rate, including the nucleation, on nylon 6 increased after nano-composite formation as compared with that of the neat nylon 6.

The formation of the network structure owing to the dispersed MMT particles affected the lamellar growth of the γ-phase crystal.

Despite extensive studies of the polymer crystallization in nylon 6-based nano-composites, the correlation between the nucleating effect and the growth mechanism of the different polymorphism (γ-phase) underlying these observation is not very well explored in the literature. In this regard, we need to pin down the crystallization kinetics of the nylon 6-clay nano-composites.

To better understand the kinetics, time-resolved Fourier transform infrared spectroscopy (FTIR) is a very powerful tool on the basis of the change in the molecular conformation of the nylon 6 during isothermal crystallization. It motivated us to investigate the time development of the different polymorph in the nylon 6 upon nano-composite formation. Recently, a full analysis of the crystallization of nylon 6 in nano-composites has been done by using FTIR [10], but not by time-resolved FTIR analysis.

* Corresponding author. Fax: +81 (0) 52 809 1864.
E-mail address: okamoto@toyota-ti.ac.jp (M. Okamoto).

0032-3861/$ – see front matter © 2010 Elsevier Ltd. All rights reserved.
doi:10.1016/j.polymer.2010.09.033

In the present paper, *via* time-resolved FTIR, we examined the real-time investigation of the change in the molecular conformation of the nylon 6 during crystallization of neat nylon 6 and the corresponding nano-composite. Knowledge of such a comparison should also be useful in assessing how does the nano-filler control the crystallization behavior and the different polymorphism of nylon 6 matrix in the clay-based nano-composites?

2. Experimental section

2.1. Materials

The nylon 6-based nano-composite was kindly supplied by Dr. A. Usuki of Toyota Central R&D Labs., Inc. It was synthesized by *in-situ* polymerization of ε-caprolactam in lauryl ammonium intercalated MMT in the presence of small amount of 6-aminocaproic acid (the number- and weight-average molecular weights M_n and M_w of N6C3.7 are 19.7×10^3 g/mol, and 45.0×10^3 g/mol, respectively) [9]. The amount of inorganic montmorillonite (MMT) part, obtained from the burning out of organic part, was 3.7% and was designated as N6C3.7. The M_n and M_w of pure nylon-6 polymerized in bulk were 21.7×10^3 g/mol and 44.0×10^3 g/mol, respectively.

The nano-composite structure of N6C3.7 exhibited well-exfoliated structure. Details regarding the structure analysis can be found in our previous paper [12].

2.2. Differential scanning calorimetry (DSC)

The crystallized specimens were characterized by using temperature-modulated DSC (TMDSC) (TA 2920; TA Instruments) at the heating/cooling rate of 5 °C/min with a heating/cooling cycle of the modulation period of 60s and an amplitude of +/−0.769 °C, to determine the crystallization temperature with cooling from melt (T_{cc}), the melting temperature (T_m) and heat of fusion (ΔH), the DSC was calibrated with Indium before experiments. For the measurement of degree of crystallinity (χ_c) prior to TMDSC analysis, the extra heat absorbed by the crystallites formed during heating had to be subtracted from the total endothermic heat flow due to the melting of the whole crystallites. This can be done according to the principles and procedures described in our previous paper [18]. In the TMDSC experiments, the endothermic heat flow $\Delta H_{\text{different}}$ of the initially existing crystallites can be easily calculated as $\Delta H_{\text{difference}} = \Delta H_{\text{rev}} - \Delta H_{\text{nonrev}}$, where ΔH_{rev} is the endothermic melting (reversible) enthalpy from the reversing heat flow profile and ΔH_{nonrev} is the exothermic ordering/crystallization (nonreversible) enthalpy from the nonreversing heat flow profile appearing in the temperature range of 150–230 °C.

By considering the melting enthalpy of 100% crystalline nylon 6 (α-phase as 241 J/g and γ-phase as 239 J/g, respectively [19]), we have estimated the value of the χ_c, calculated as $\Delta H_{\text{difference}}/\Delta H_{100\%}$, of neat nylon 6 and N6C3.7, and these values are also presented in Table 1.

2.3. Fourier transform infrared spectroscopy (FTIR)

FTIR spectra were collected at 2 cm^{-1} nominal resolution using a Varian FTS7000 spectrometer equipped with an MCT detector in transmission mode. The spectra were obtained by averaging 32 scans with a mean collection length of 0.6 s per spectrum. The background spectra used for reduction were collected at the same crystallization temperature (T_c) with the sample. The homogenous mixture of KBr powder and nylon 6 (powder) or N6C3.7 (powder) in the weight ratio 98:2 was prepared. The mixtures were then converted into disks with a thickness of ~0.4 mm by pressing. We have used homemade heating/cooling chamber with a cooling rate of ~1000 °C/min. The disks were placed in a homemade environmental heating chamber, which allowed to reach the desired T_c in a very short time (~2 s). Each sample was kept at 250 °C for 5 min to erase any thermal history, and it was immediately cooled to T_c. After attaining the T_c, a time-resolved FTIR measurement was carried out in the temperature range of 150–195 °C. The collected data were processed by soft ware (Grams/AI®, Thermo Galactic Co., USA).

Table 1
TMDSC properties of neat nylon6 and its nano-composite.

Samples	T_{cc}/°C	T_m/°C	ΔH_{rev}/J/g	ΔH_{nonrev}/J/g	ΔH_{diff}/J/g	χ_c/%
Nylon 6	176.2	221.5	80.0	15.0	65.0	27.0
N6C3.7	186.0	215.4	57.1	2.9	54.2	22.7

3. Results and discussion

3.1. Crystallization behavior

Fig. 1 shows the TMDSC thermograms of neat nylon 6 and N6C3.7 during cooling from melt state (~260 °C) and 2nd heating with a rate of 5 °C/min. For N6C3.7, the evolution of the crystallization peak is sharp and its maximum is at 186 °C. For the neat nylon 6, this peak is much broader and it appears at 176 °C. The dispersed MMT particles in N6C3.7 promote the crystallization possibly due to the nucleation effect. The estimate values of χ_c are shown in Table 1. The presence of MMT particles cause a slight shift in the melting peak to slightly lower temperature (215.4 °C) and lower total crystallinity. In our previous observation [9], the lower T_m has been attributed to an increased fraction of γ–phase crystallites present in N6C3.7. As seen in Table 1, the higher T_{cc} value for N6C3.7 (T_{cc} = 186.0 °C) suggests that the nano-composite is more easily crystallizable as compared with neat nylon 6 (T_{cc} = 176.2 °C) during the TMDSC cooling process.

3.2. Spectral evolution during crystallization

Fig. 2(a–c) and Fig. 3(a–c) show a typical time-dependent spectral variations of neat nylon 6 and the corresponding nano-

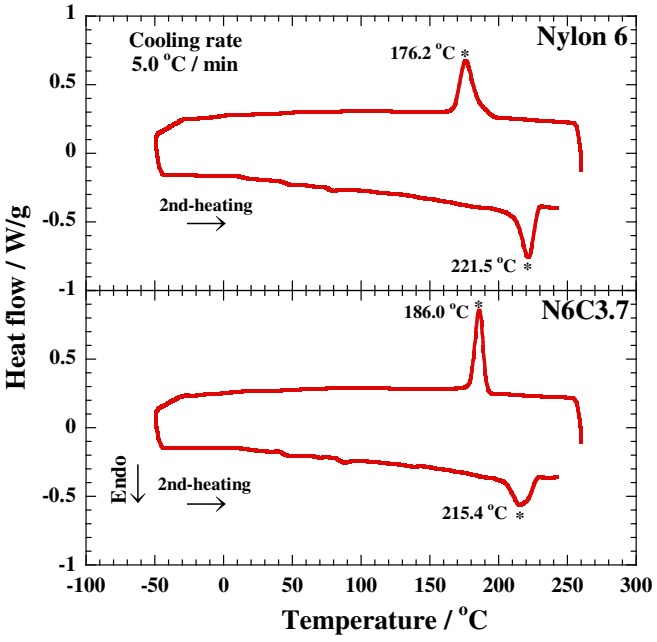

Fig. 1. TMDSC scan for neat nylon 6 and its nano-composite (N6C3.7).

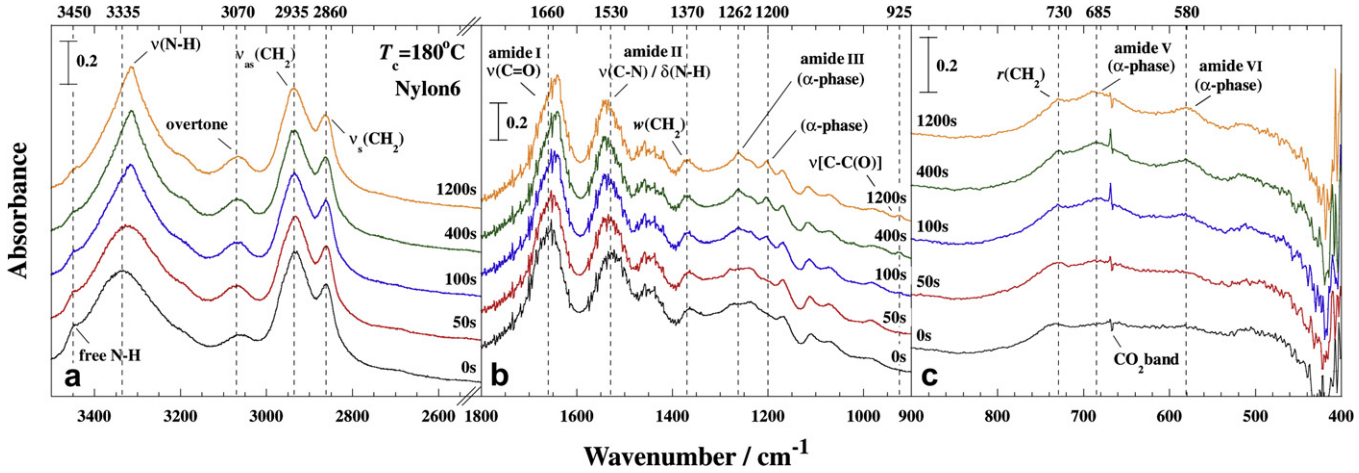

Fig. 2. Time-resolved spectra in the region of (a) 3500–2600 cm^{-1}, (b) 1800–900 cm^{-1} and (c) 900–400 cm^{-1} during isothermally crystallization of neat nylon 6 at 180 °C for 1200 s. The data in the *y*-axis direction was shifted to avoid data overlap.

composites (N6C3.7) in the region of 3500–400 cm^{-1} during isothermal crystallization at 180 °C for neat nylon 6 and at 158 °C for N6C3.7. The frequencies and the vibrational assignments for the neat nylon 6 with α–phase and nano-composites with γ–phase are reported in the literature [10]. In Fig. 2(a), a band located at 3450 cm^{-1}, which is assigned to the hydrogen bond-free N–H stretching mode, arise and their intensities decrease until the crystallization is complete (~1200 s). The time variation of the band at 3335 cm^{-1} (attributed to the hydrogen bonded N–H stretch: some times called amide A) provides valuable information. This amide A band shifts to the lower frequency side and changes to sharper peak with crystallization time, reflecting the formation of the intermolecular hydrogen bonding. At the same time, hydrogen bond-free band at 3450 cm^{-1} decreases in intensity. The band of around 3070 cm^{-1}, which is overtone of the amide bonding, shifts oppositely to the higher frequency side, indicating the enhancement of the intermolecular hydrogen bond strength. That is to say, the crystallization takes place.

The bands at 2935 (asymmetric methylene stretching mode: $\nu_{as}(CH_2)$) and 2860 cm^{-1} (symmetric methylene stretching mode: $\nu_s(CH_2)$) are not related to crystalline fraction [10]. These bands are discussed in terms of the conformational change and lateral chain–chain interaction [20].

The α-phase shows characteristic absorbance peaks at ca. 1660 (amide I: ν(C=O)), 1530 (amide II: coupling of C–N stretching and N–H in plane bending), 1262 cm^{-1} (amide III) and 1200 cm^{-1} as seen in the region from 900 to 1800 cm^{-1} (Fig. 2(b)). The bands at 1370 and 925 cm^{-1} are CH_2 wagging vibration and intrinsic band to CH_2CO group, respectively. The region from 400 to 900 cm^{-1} is shown in Fig. 2(c). The amide V((N–H) wagging mode; w(N–H)) and amide VI ((C=O) wagging mode; *w*(C=O)) bands appear at 685 and 580 cm^{-1} respectively, for the characteristic of α-phase. The band at 730 cm^{-1} corresponds to the rocking mode of CH_2. Both α- and γ-phases show this band at the same wave number, indicating the same conformation of CH_2 segments when the different hydrogen bonding schemes are taken place.

Qualitatively, the spectra of the γ-phase look similar, but the peak occurs at 625 cm^{-1} (amide VI), which is shifted from 580 cm^{-1} for α-phase (Fig. 3(c)). An interesting feature is the contribution to the amide III, which comes from bands at 1232 cm^{-1} for the γ-phase and 1262 cm^{-1} for the α-phase [10] (Fig. 3(b)). These results suggest that major γ-phase crystal coexist with small α-phase is formed in the nano-composite systems, while neat nylon 6 predominantly forms α-phase despite of the evolution of the sequence in the amide III. Another interesting feature is the amide A band. The amide A band for the α–phase is sharper than the

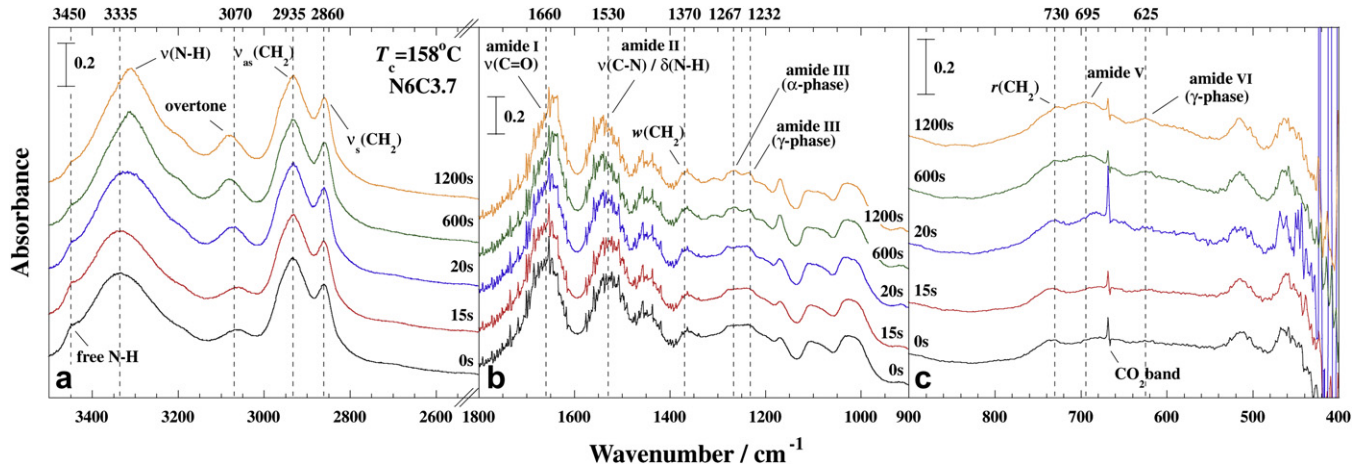

Fig. 3. Time-resolved spectra in the region of (a) 3500–2600 cm^{-1}, (b) 1800–900 cm^{-1} and (c) 900–400 cm^{-1} during isothermally crystallization of N6C3.7 at 158 °C for 1200 s. The data in the *y*-axis direction was shifted to avoid data overlap.

γ-phase after the crystallization is complete (see Fig. 3(a)). In the case of N6C3.7, the bands at around 1020 and 463 cm^{-1} are due to Si–O stretch of the MMT layers [21].

3.3. Time-dependent spectral evolution

Figs. 4 and 5 show typical examples of the time variation of the reduced intensities for the characteristic bands taken at 167 °C and 158 °C for neat nylon 6 and for N6C3.7, respectively. The upper panels in each figure indicate the temperature drop profile during crystallization of the sample. During the temperature drop of the sample, a very rapid temperature change is observed till the achievement of T_c (~1500 °C/min). The T_cs were chosen by referring to the equilibrium melting temperature ($T_m°$). The values of T_m by Hoffman-Weeks [22] extrapolation based on plotting T_m versus T_c were 221.2 °C for neat nylon 6 and 215.8 °C for N6C3.7 [12].

The absorbance of the 2220 cm^{-1} band is regarded as an internal standard because no change was observed during crystallization process. Therefore, the intensity of crystalline-sensitive bands and the internal standard is used to depict the crystalline structure development.

For neat nylon 6 at T_c = 167 °C (supercooling (ΔT) (=$T_m - T_c$) (≅54.2 °C)), we notice that for the amide A band, the intensity growth and frequency shift to the lower side are very rapid as compared with the intensity changes of the hydrogen bond-free and amide III bands (Fig. 4(a)). This feature is also observed in the temperature range of 155–195 °C for neat nylon 6 crystallization. After the temperature drop to T_c, in an early stage the stronger hydrogen bonding interactions are formed as revealed by a ν(N–H) band intensity increment. The formation of α-phases appear at much later timing. The neat nylon 6 predominantly forms α-phase in the T_c range of 155–195 °C.

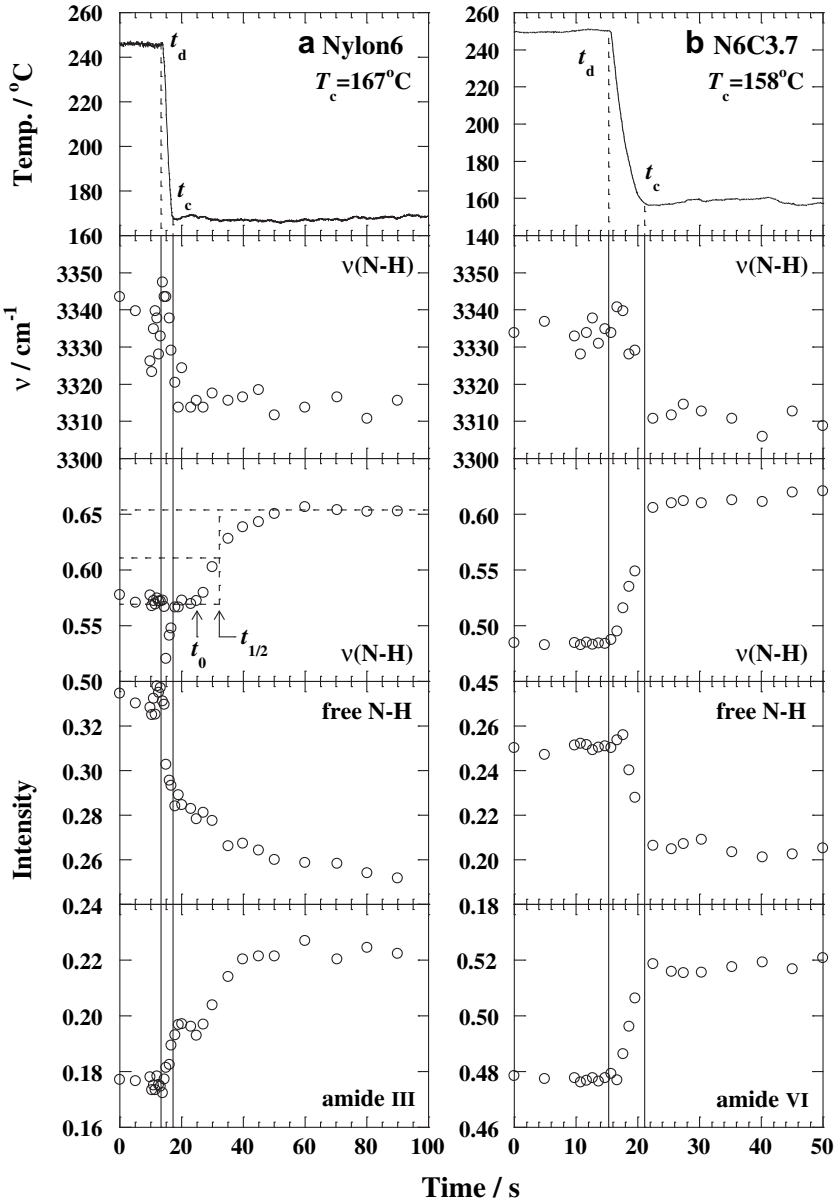

Fig. 4. Time variation of intensity for crystalline-sensitive bands of (a) neat nylon 6 taken at 167 °C and (b) N6C3.7 taken at 158 °C. Upper panels indicate temperature drop profile during crystallization of the sample. The arrows indicate the induction time (t_0) of crystallization and the crystallization *half-time* ($t_{1/2}$). The broken lines indicate onset time of temperature drop (t_d) and onset time of isothermal crystallization (t_c) (see text for details).

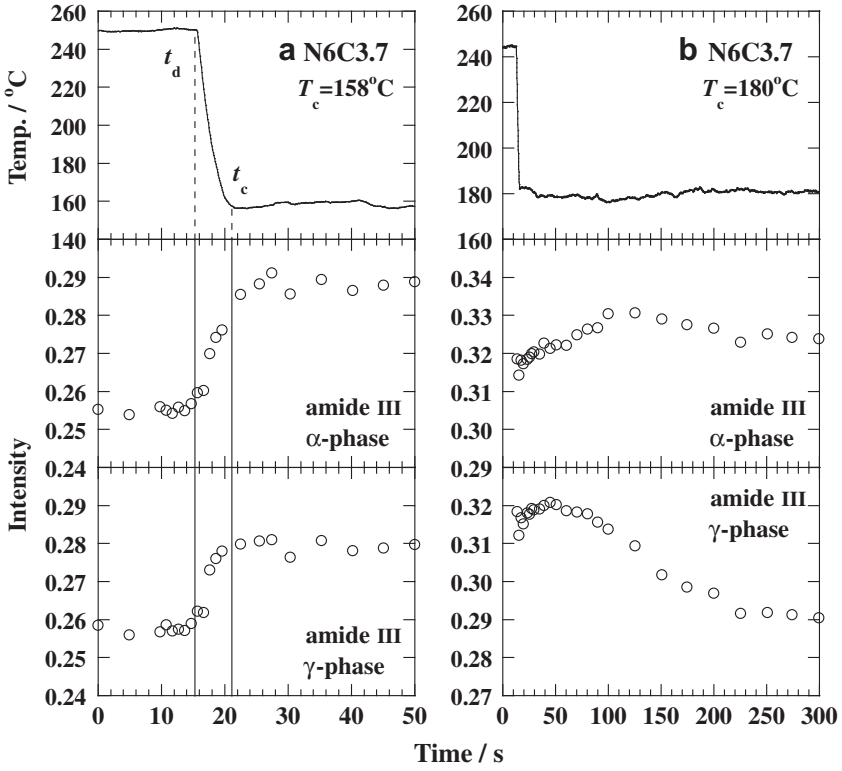

Fig. 5. Time variation of intensity for crystalline-sensitive bands of N6C3.7 taken at (a) 158 °C and (b) 180 °C. Upper panels indicate temperature drop profile during crystallization of the sample.

For N6C3.7 at $T_c = 158$ °C ($\Delta T \cong 57.8$ °C) (Fig. 4(b)), just after the temperature drop, the intensity growth for all characteristic bands and frequency shift of ν(N–H) band take place abruptly during rapid cooling from onset time of temperature drop (t_d) to onset time of isothermal crystallization (t_c). It is very clear that we cannot estimate the onset time (t_0) until start of crystallization. The same trend is also observed in low T_c range of 150–168 °C ($\Delta T = 47.8$–65.8 °C). Therefore it can be assumed that the dispersed MMT particles induce epitaxially crystallized chain growth on their surfaces as a nucleating agent (heterogeneous nucleation). Another interesting feature is the formation of α-phase over the wide range of ΔT studied here (Fig. 5(a) and (b)). For the amide III bands, the region is broad to deconvolute meaningfully into individual peaks and hence is discussed as a composite peak and provides valuable information. N6C3.7 exhibits mainly γ-phase crystal coexisting with α-phase at low T_c range (=150–168 °C), owing to the dispersed MMT particles, as revealed by wide-angle X-ray diffraction (WAXD) analysis [12]. A major α-phase crystal coexists with γ-phase appeared at high T_c range (=177–191 °C). The intensity of amide III band of γ-phase first increases and then decreases beyond 50 s to reach constant intensity. This result suggests that the crystalline phase transition from γ-phase to α-phase was occurred. The phase transition prior to melting is considered due to temperature variation and packing change within the crystal. Only the part less influenced by the dispersed MMT particles can undergo phase transition effectively. This feature has already been observed in the temperature dependence of the crystallinity degree of the α-phase by Liu et al. [24].

As shown in Fig. 4(a), we estimated the induction time (t_0) and the crystallization *half-time* $t_{1/2}$ at which the reduced intensity reaches 1/2, we define $1/t_{1/2}$ as a measure of the overall crystallization rate at each characteristic band [23].

In Fig. 6, at all T_c measured here the t_0 value of ν(N–H) band of N6C3.7 is lower than that of neat nylon 6. In the changes in t_0 with ΔT (= 24.8–38.8 °C), the N6C3.7 shows no induction time especially at large ΔT (= 47.8–65.8 °C), suggesting that the dispersed MMT particles have a significant contribution to enhance the nucleation of the γ-phase crystal as mentioned above. This is due to the formation of the network structure owing to the dispersed MMT particles affected the mobility of nylon molecular chains. At

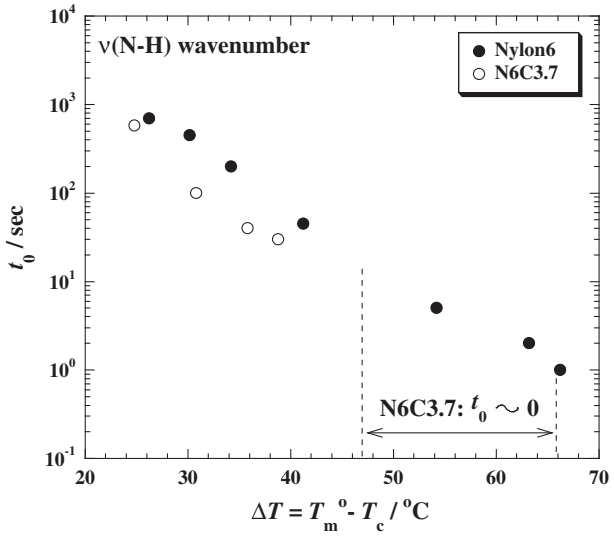

Fig. 6. ΔT dependence of induction time of of ν(N–H) band for neat nylon 6 and N6C3.7. N6C3.7 shows no induction time especially at large ΔT (=47.8–65.8 °C) (see text for details).

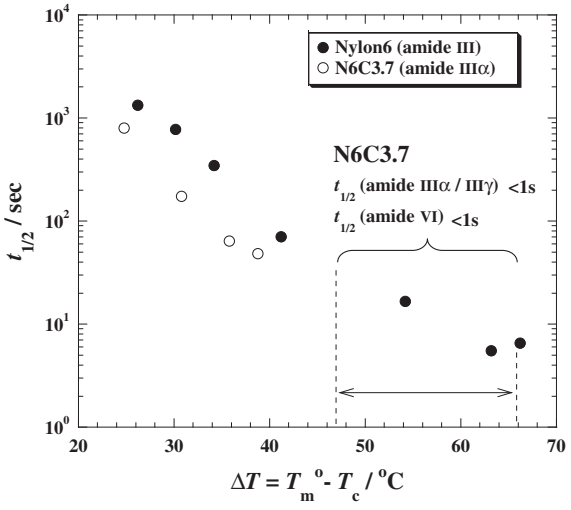

Fig. 7. Δ*T* dependence of crystallization *half-time* of different polymorphs (amide III for neat nylon 6 and amides IIIα, IIIγ and VI for N6C3.7).

T_c = 150–168 °C the crystallization with large Δ*T* provides the disturbed crystal growth and hinder the stable growth of the α-form due to the lack of time for crystalline structure development. The formation of hydrogen bonded sheets of the γ-phase is dominant as reported by our previous study [12]. On the other hand, the stable growth of the α-phase crystal occurred at high T_c range (Δ*T* = 24.8–38.8 °C). This feature is also observed in the temperature dependence of the crystallization rate (see Fig. 7).

In Fig. 7, we constructed a plot of $t_{1/2}$ versus Δ*T* the growth behavior of the different polymorphs in the nylon 6 upon nanocomposite formation. For the bands of amides IIIα, IIIγ and VI of N6C3.7, the crystallization takes place so rapidly (less than 1 s) as compared with that of amide III of neat nylon 6 at low T_c range of 150–168 °C (Δ*T* = 47.8–65.8 °C). Here, the network structure still affected chain folding, resulting in the formation of the γ-phase, but chain mobility at elevated temperatures is comparable to neat nylon 6 as demonstrated by the temperature dependence of the overall crystallization rate.

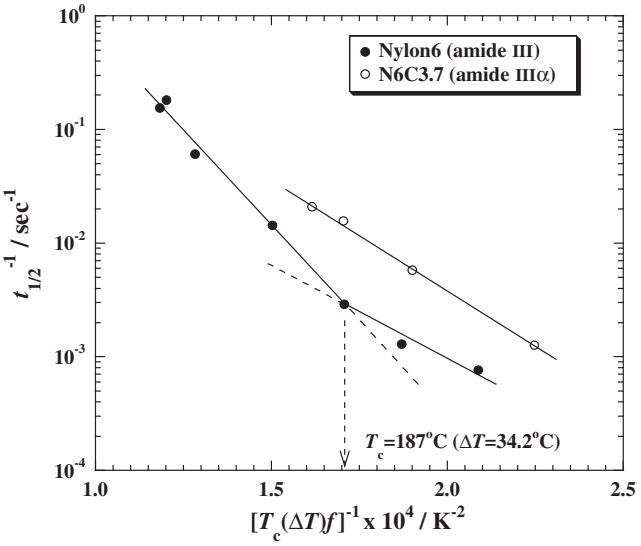

Fig. 8. The plot of overall crystallization rate versus $1/(T_c\Delta Tf)$ for different T_cs in amide III band for neat nylon 6 and amide IIIα band for N6C3.7. The broken line indicates $1/(T_c\Delta Tf) = 1.71 \times 10^{-4}$ K^{-2} (T_c = 187 °C).

In order to analyze the crystallization growth rate, we assume heterogeneous nucleation and apply the Hoffman–Lauritzen growth rate equation of slow kinetics [25,26] even if we are not using the analysis to determine linear growth rates. The growth rate of crystal can be written as

$$\text{Overall rate} \propto \beta_g \exp\left[-\frac{K_g}{T_c(\Delta T)f}\right] \quad (1)$$

where β_g is a mobility term, which describes the transportation rate of crystallizable molecules to the growth front; *f* is the correction factor given by $2T_c/(T_m + T_c)$; and K_g is the nucleation constant, which depends on the crystallization regimes (regime I, single nucleation; regimes II and III, multiple nucleation) [25,27]. At small supercoolings and over limited temperature range, the temperature dependence of growth is determined predominantly by the nucleation term. Accordingly, assuming that the $1/t_{1/2}$ is a satisfactory measure to the rate of crystallization, we plot the data as $1/t_{1/2}$ versus $1/(T_c\Delta Tf)$: see Fig. 8.

The overall rate of amide IIIα band for N6C3.7 is enhanced for every temperature of measurement as compared with that of amide III for neat nylon 6. The result obviously implies that the number of nucleation sites is larger in N6C3.7, but the growth mechanism in the subsequent crystallization processes are virtually the same in both nano-composite and neat nylon 6 because of almost same slope (~4 × 10^4 K^2), reflecting the apparent nucleation constant. As discussed in the beginning in Fig. 7, unfortunately, we could not discuss the crystallization kinetics of amides IIIγ and VI for N6C3.7 for a small Δ*T* range.

For neat nylon 6 crystallization, a change in slope at $1/(T_c\Delta Tf) \cong 1.71 \times 10^{-4}$ K^{-2} corresponding to Δ*T* ≅ 34.2 °C (T_c ≅ 187 °C) is obvious. The ratio of the two slopes is about 2, suggesting a transition from regime III to regime II at T_c ≅ 187 °C [27].

4. Conclusions

We have investigated the change in the molecular conformation of the nylon 6 during crystallization of neat nylon 6 and the corresponding nano-composite (N6C3.7) having well-exfoliated structure. The neat nylon 6 predominantly formed α-phase in the crystallization temperature (T_c) range of 155–195 °C N6C3.7 exhibited mainly γ-phase crystal coexisting with α-phase at low T_c range (=150–168 °C). It was shown that for the bands of amides IIIα, IIIγ and VI for N6C3.7, the crystallization took place so rapidly (less than 1 s) without induction time of crystallization as compared with that of amide III for neat nylon 6 at low T_c range of 150–168 °C (Δ*T* = 47.8–65.8 °C). Here, the network structure still hindered chain folding, resulting in the formation of the γ-phase, but the chain mobility at elevated temperatures (T_c = 177–191 °C) was comparable to the neat nylon 6 as demonstrated by the temperature dependence of the overall crystallization rate. The growth mechanism in the subsequent crystallization processes (amides IIIα and IIIγ) was virtually the same in both nano-composite and neat nylon 6. The number of nucleation sites was larger in N6C3.7 as compared with that of neat nylon 6. The dispersed MMT particles strongly contributed toward the enhancement of heterogeneous nucleation, leading to the formation of both α- and γ-phase crystals during the crystallization of N6C3.7.

Acknowledgment

This work was supported by the MEXT "Collaboration with Local Communities" Project (2005–2009).

References

[1] Kojima Y, Usuki A, Kawasumi M, Okada A, Fukushima Y, Kurauchi T, et al. Mater Res 1993;8:1185.
[2] Kojima Y, Usuki A, Kawasumi M, Okada A, Kurauchi T, Kamigaito O, et al. J Polym Sci Part B Polym Phys 1994;32:625.
[3] Mathias L, Davis R, Jarrett W. Macromolecules 1999;32:7958.
[4] Lincoln DM, Vaia RA, Wang ZG, Hsiao BS. Polymer 2001;42:1621.
[5] VanderHart DL, Asano A, Gilman JW. Chem Mater 2001;13:3781.
[6] Lincoln DM, Vaia RA, Wang ZG, Hsiao BS, Krishnamoorti R. Polymer 2001;42:9975.
[7] Medellin-Rodriguez FJ, Burger C, Hsiao BS, Chu B, Vaia RA, Phillip S. Polymer 2001;42:9015.
[8] Kamal MR, Borse NK, Garcia-Rejion A. Polymer Eng Sci 2002;42:1883.
[9] Maiti P, Okamoto M. Macromol Mater Eng 2003;288:440.
[10] Nair SS, Ramesh C. Macromolecules 2005;38:454.
[11] Bertmer M, Wang M, Kruger M, Blumich B, Litvinov VM, van Es M. Chem Mater 2007;19:1089.
[12] Kato Y, Okamoto M. Polymer 2009;50:4718.
[13] Holes DR, Bunn CW, Smith DJ. J Polym Sci 1955;17:159.
[14] Fornes TD, Paul DR. Polymer 2003;44:3945.
[15] Homminga DS, Goderis B, Mathot VBF, Groeninckx G. Polymer 2006;47:1630.
[16] Miltner HE, Van Assche G, Pozsgay A, Pukanszky B, Van Mele B. Polymer 2006;47:826.
[17] Wang K, Liang S, Deng J, Yang H, Zhang Q, Fu Q, et al. Polymer 2006;47:7131.
[18] Nam PH, Maiti P, Okamoto M, Kotaka T, Hasegawa N, Usuki A. Polymer 2001;42:9633.
[19] Illers KH. Makromol Chem 1978;179:497.
[20] Jakes J, Krimm S. Spectrochim Acta 1971;27A:35.
[21] Loo LS, Gleason KK. Macromolecules 2003;36:2587.
[22] Martuscelli E, Silvestre S, Abate G. Polymer 1982;23:229.
[23] Asai K, Okamoto M, Tashiro K. Polymer 2008;49:5186.
[24] Liu X, Wu Q. Polymer 2002;43:1933.
[25] Lauritzen JI, Hoffman JD. J Appl Phys 1973;44:4340.
[26] Hoffman JD, Froln LJ, Ross GS, Lauritzen JI. J Res Natl Bur Stand (A) 1975;79:671.
[27] Hoffman JD. Polymer 1983;24:3.